SANDIA REPORT

SAND2016-11328
Unlimited Release
Printed October 2016

Development of Scanning Ultrafast Electron Microscope Capability

Kimberlee C. Collins, David W. Chandler, A. Alec Talin, Joseph R. Michael

Prepared by
Sandia National Laboratories
Albuquerque, New Mexico 87185 and Livermore, California 94550

Sandia National Laboratories is a multi-mission laboratory managed and operated by Sandia Corporation, a wholly owned subsidiary of Lockheed Martin Corporation, for the U.S. Department of Energy's National Nuclear Security Administration under contract DE-AC04-94AL85000.

Issued by Sandia National Laboratories, operated for the United States Department of Energy by Sandia Corporation.

Available to DOE and DOE contractors from
U.S. Department of Energy
Office of Scientific and Technical Information
P.O. Box 62
Oak Ridge, TN 37831

Telephone: (865) 576-8401
Facsimile: (865) 576-5728
E-Mail: reports@osti.gov
Online ordering: http://www.osti.gov/scitech

Available to the public from
U.S. Department of Commerce
National Technical Information Service
5301 Shawnee Rd
Alexandria, VA 22312

Telephone: (800) 553-6847
Facsimile: (703) 605-6900
E-Mail: orders@ntis.gov
Online order: http://www.ntis.gov/search

SAND2016-11328
Unlimited Release
October 2016

Development of Scanning Ultrafast Electron Microscope Capability

Kimberlee C. Collins, A. Alec Talin
Materials Physics
Sandia National Laboratories
P.O. Box 969
Livermore, CA 94551-MS9161

David W. Chandler
Chemical, Combustion and Materials Center
Sandia National Laboratories
P.O. Box 969
Livermore, CA 94551-MS9054

Joseph R. Michael
Materials Science and Engineering
Sandia National Laboratories
P.O. Box 5800
Albuquerque, New Mexico 87185-MS0886

Abstract

Modern semiconductor devices rely on the transport of minority charge carriers. Direct examination of minority carrier lifetimes in real devices with nanometer-scale features requires a measurement method with simultaneously high spatial and temporal resolutions. Achieving nanometer spatial resolutions at sub-nanosecond temporal resolution is possible with pump-probe methods that utilize electrons as probes. Recently, a stroboscopic scanning electron microscope was developed at Caltech, and used to study carrier transport across a Si p-n junction [1,2,3]. In this report, we detail our development of a prototype scanning ultrafast electron microscope system at Sandia National Laboratories based on the original Caltech design. This effort represents Sandia's first exploration into ultrafast electron microscopy.

ACKNOWLEDGMENTS

Numerous individuals at Sandia National Laboratories contributed to the completion of this project. In particular, we extend our gratitude to the contributions of Mark Jaska, Josh Whaley, Kenneth Stewart, Charles Steinhaus, David Heredia, Elliot Fuller, Patrick Feng, Meredith Anderson, Todd Felver, Amanda Cervantez, Suzy Vitale, and Nicole Kohrs. We also received helpful input from Scanservice Corp. and Fianium. Finally, we thank Professor Ding-Shyue Yang for his invaluable consultations.

CONTENTS

FIGURES

1. INTRODUCTION

The operation of most modern semiconductor devices such as photodetectors, laser diodes, photovoltaics and transistors, depends on the injection and transport of minority carriers across different device regions with dimensions ranging from millimeters to nanometers. Imaging these regions with high spatial resolution and simultaneously capturing the dynamics of carrier transport with high temporal resolution has been a long standing goal of device engineers and physicists [4]. Electron beam methods such as electron beam induced current (EBIC) or secondary electron contrast can image space-charge regions in a semiconductor device, which can then be related to dopant concentration. Additionally, Kelvin probe force microscopy (KPFM) can also image space-charge regions by measuring changes in the surface potential. None of these techniques, however, provides any information regarding carrier dynamics. Optical pump-probe spectroscopy or time-resolved photoluminescence (TRPL) can measure carrier lifetime and recombination rates with femtosecond resolution, but are diffraction limited to hundreds of nanometers, and typically have spatial resolutions of hundreds of micrometers. Because of their limited spatial resolution, the purely optical time resolved methods cannot image carrier dynamics in many realistic devices structures nor around specific structural defects such as dislocations, voids and grain boundaries.

The quantification of lifetimes in real devices can also provide insights into doping carrier concentration. Figure 1 shows reported minority carrier lifetimes in Si and GaN for both p- and n-type materials as a function of majority carrier concentration [5,6,7,8]. Fast detection schemes are limited to ~1 ns temporal resolution, so measuring lifetimes on that order or shorter requires pump-probe laser-based methods which are temporally limited by laser pulse width rather than detection electronics. Unlike Si, which has exceptionally long lifetimes, GaN, which is an important wide band gap material in areas like solid-state lighting and power electronics, has exceptionally short lifetimes. To study GaN or highly doped Si, sub-ns temporal resolutions are needed.

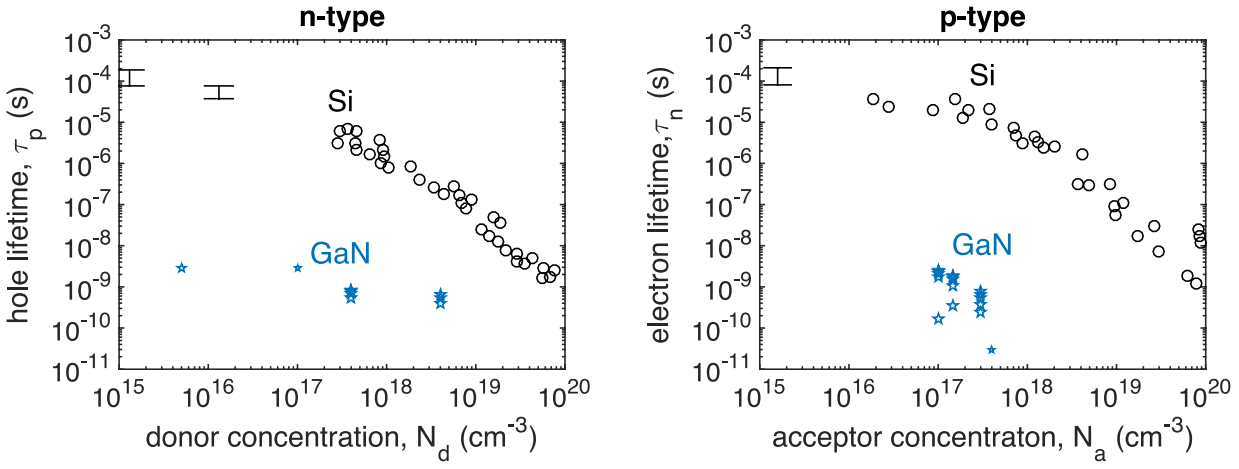

Figure 1. Minority carrier lifetimes in Si and GaN as a function of doping concentration[5] [6] [7] [8].

Our approach for lifetime measurements with high spatial resolution was to implement scanning ultrafast electron microscopy (S-UEM), a stroboscopic time-resolved SEM system first developed by Zewail and coworkers at Caltech [1,2]. S-UEM, which is an SEM-based system, has advantages over time-resolved TEM systems with regards to measuring bulk samples [1]. This report details our efforts to implement a S-UEM system at Sandia National Laboratories. This represents Sandia's first exploration into ultrafast electron microscopy.

1.1. A brief overview of ultrafast electron microscopy

Ultrafast electron microscopy methods have been developed since the 1970s [9] to study transient phenomena with higher time resolution than afforded by fast detectors [10]. Typically ultrafast methods are aimed at time scales <1 ns, and achieve this with pump-probe arrangements. In ultrafast electron microscopy, electrons are used as probes, rather than the conventional all-optical pump-probe setup. Electrons can be focused below the diffraction limit for optical wavelengths, thus can enable measurements with simultaneously high spatial and temporal resolution, beyond the capability of all-optical systems. Two main classes of ultrafast electron microscopes have been developed: single-shot and multi-shot systems. Single-shot systems collect full images or diffraction patterns with a single, high brightness electron pulse and are capable of measuring non-repeatable processes, while multi-shot systems build an image from many low brightness electron pulses and rely on the repeatability of the studied dynamics.

1.1.1. Single-shot methods

Single-shot ultrafast electron microscope systems capture full images or diffraction patterns from a single optical excitation pulse (pump) and a single, bright pulse of electrons (probe) with a delayed arrival time. The dynamics corresponding to the set delay time are recorded, and the experiment is repeated at subsequent delays to form a transient data set. The advantage of single-shot methods over multi-shot methods is their ability to study highly irreversible processes such as solid-to-liquid phase transitions. A disadvantage of single-shot methods is lower spatial and temporal resolutions due to the large number of electrons required for single-shot imaging, which leads to columbic broadening of the electron pulse.

One notable single-shot electron microscope is the dynamic transmission electron microscope (DTEM) [11,12]. The DTEM uses a pulsed laser to generate a bright electron pulse from a TEM cathode. The electron pulse is bright enough to collect a full TEM image (~1e9 electrons per pulse), and is preceded by an optical excitation pulse that perturbs the sample. The excited physics can be highly irreversible, such as melting or ablation [13]. A set of time-resolved data can be collected for an irreversible process by moving to a new sample location and repeating the measurement. Alternatively, a series of electron probe pulses can be generated following each pump pulse to capture several time frames after a single excitation [14]. The DTEM's focus on direct imaging eliminates the need to invert a diffraction pattern, and the time resolution greatly exceeds TEM video capture rates which are on the order of milliseconds. The large number of electrons per pulse requires modifications to the electron column, and limits the spatial resolution to ~10 nm and the temporal resolution to ~15 ns [12]. A schematic illustration of a direct imaging DTEM is shown in Figure 2a.

Sub-ps time resolution in near-single-shot measurements has been achieved through custom photoactivated electron guns with extremely compact designs that minimize the propagation time available for electron pulse broadening, a method pioneered by Miller and coworkers [15,16,17,18]. These setups utilize thin samples and measure the diffraction pattern of transmitted electrons. They have demonstrated <200 fs time resolution with near-single-shot diffraction imaging of order-to-disorder phase transitions [16,17].

1.1.2. Multi-pulse methods

Multi-pulse pump-probe schemes are more straightforward to implement than single-shot methods, often requiring no modifications to conventional electron microscope optics. Multi-pulse methods also provide superior temporal and spatial resolutions by reducing the number of electrons per pulse and hence minimizing space-charge broadening. One drawback of multi-pulse methods is that they are limited to highly repeatable dynamics. With only a few electrons per pulse, more than 1e6 pulses may be required to form a full image or diffraction pattern with reasonable signal-to-noise.

The multi-pulse analogue to DTEM is four-dimensional ultrafast electron microscopy (4D UEM), a method developed by Zewail and coworkers [19,20], building upon earlier multi-pulse TEM systems [9]. 4D UEM is illustrated schematically in Figure 2b. Low brightness electron pulses (~1 electron per pulse) are generated from a TEM cathode with a high repetition rate laser, which is also used to pump the sample. The arrival time of the optical pump and electron probe pulse chains is controlled by varying their respective path lengths. For each delay time, many (>1e6) pulses are used to generate a full TEM image, and a collection of delay time images forms a TEM movie. No modifications to the electron column optics are required beyond integration of the excitation laser. The 4D UEM has ~1 nm spatial resolution and sub-ps time resolution.

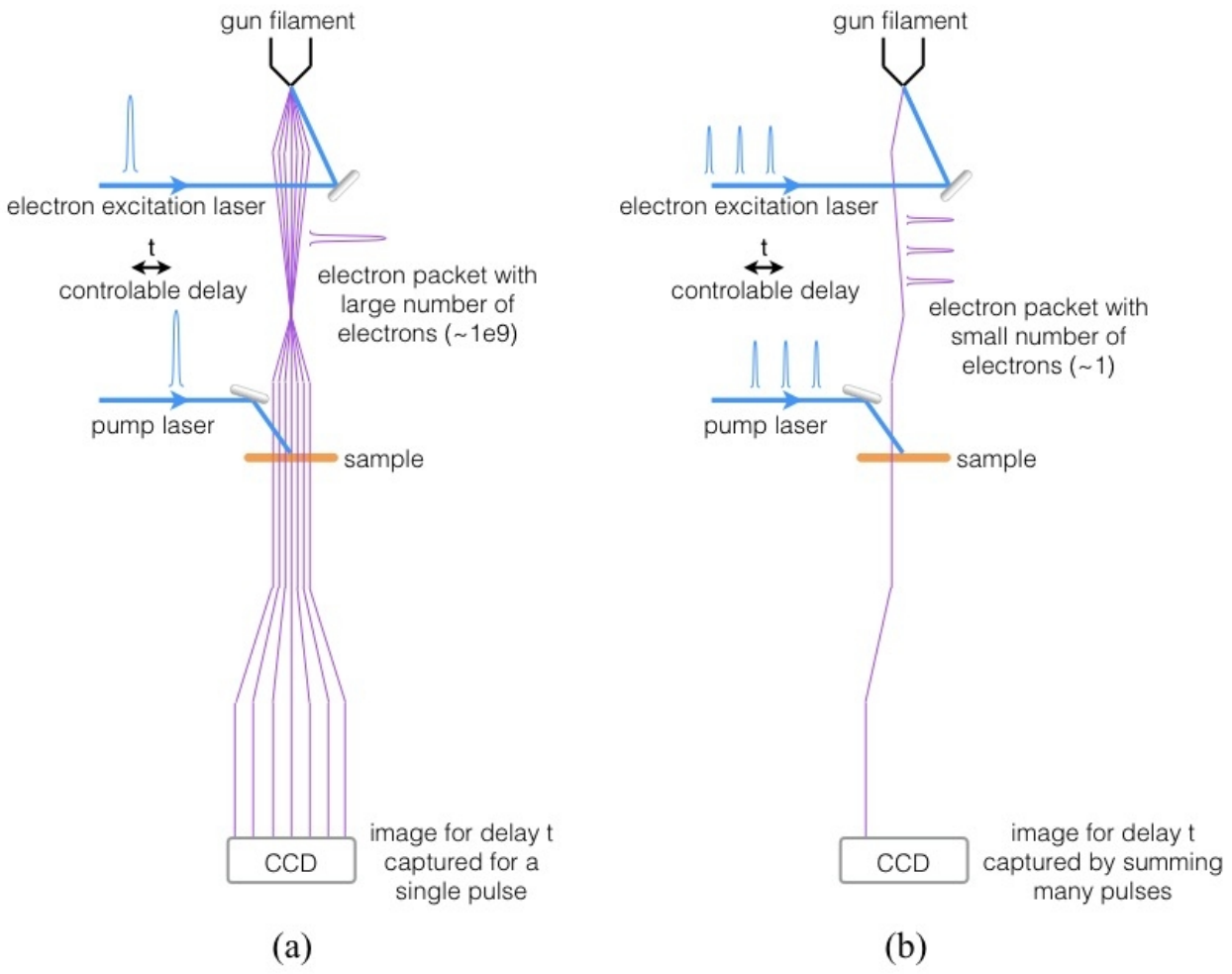

Figure 2. Conceptual diagram of time-resolved TEM methods: Comparison of (a) single-shot verses (b) multi-pulse imaging.

1.2. Prior work on scanning ultrafast electron microscopy (S-UEM)

Scanning ultrafast electron microscopy (S-UEM) was developed by Zewail and coworkers as an extension on their 4D UEM work [1,2]. Both S-UEM and 4D UEM are pump-probe time-resolved electron microscopes, but S-UEM is based on an SEM rather than a TEM. Like 4D UEM, S-UEM takes a multi-pulse approach to time-resolved imaging. A schematic illustration of a S-UEM is shown in Figure 3. A pulsed laser photoexcites the sharp field emission filament, generating an electron pulse synchronized to the excitation laser containing <10 electrons per pulse. A pulsed laser is also used to optically excite the sample. The respective arrival times of the optical excitation pulse train (pump) and the electron pulse train (probe) are controlled by a variable path length. A full SEM image is formed from many pulses (>1e8), allowing the e-beam to raster over the entire field-of-view at a given delay, and collecting the emitted secondary electrons (SEs). A set of delay time images forms an SEM movie. As with 4D UEM, no modifications to the electron column optics are required beyond the integration of a laser to

excite the cathode. An SEM-based system may be limited in spatial resolution as compared to a TEM-based system, but SEM's are capable of examining bulk samples.

The first S-UEM time-resolved images were captured in 2011 at Caltech [2], and an upgraded system has recently been build at KAUST [21]. Reports have claimed spatial resolutions <10 nm and temporal resolutions <1 ps [1,2,3,21,22,23], but to date, no data with simultaneously high temporal and spatial resolution has been demonstrated.

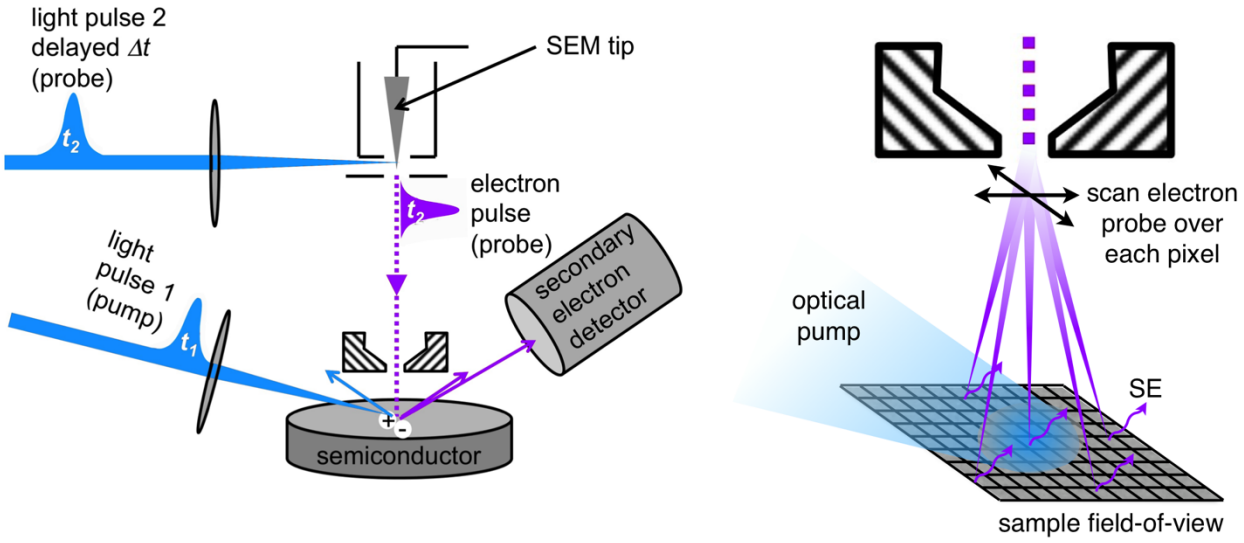

Figure 3. Conceptual diagram of pump-probe S-UEM measurements. A pulsed laser is used to excite a sample (pump) and to generate electron pulses (probe). The arrival time of the pump and probe pulse trains are controllably varied. For each time delay, the beam is scanned over each pixel to form a full SE image. The aggregate of multiple delay time images forms a SE movie.

1.3. System choice for Sandia's application space

Given Sandia's interest in studying charge carrier lifetimes in real semiconductor devices, we chose to focus our efforts on the S-UEM method. The ability to examine bulk samples, rather than thin samples which are required for TEM-based systems, was an important consideration. Additionally, we anticipated the spatial resolutions afforded by SEM would be sufficient for a large class of devices. The SEM relies on beam rastering for image formation, thus requires a multi-pulse approach to time-resolved imaging. Charge carrier excitation and relaxation is a highly repeatable process so a single-shot method was not needed. Finally, the prospect of implementing S-UEM with minimal modifications to a commercial SEM system was attractive in terms of minimizing complexity and cost.

2. SANDIA'S PROTOTYPE S-UEM SYSTEM

The objective of our efforts was to build a prototype S-UEM system to evaluate the challenges involved in implementing such a system and to examine system performance. To that end, we followed the basic model of existing multi-pulse pump-probe S-UEM systems [1,2], which couple free-space pulsed laser beams into an SEM for electron pulse (probe) generation via photoemission from a Schottky field emission filament as well as sample optical excitation (pump). The respective arrival times of the pump and probe pulse trains are controlled by a variable path length. An image is formed at a particular time delay from secondary electron emission as the primary electron beam is scanned over the sample using standard SEM optics. This process is repeated at subsequent delay times to form a secondary electron movie of the pump-excited dynamics. A basic diagram of our setup is shown in Figure 4. Below we describe our implementation in detail.

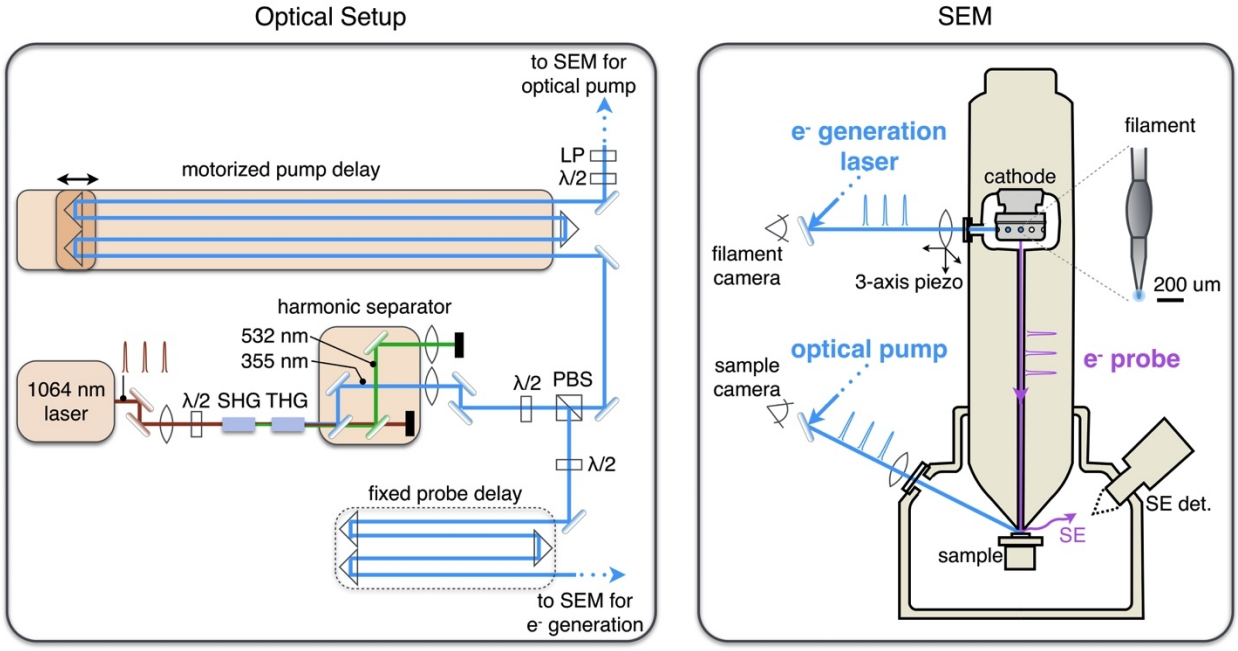

Figure 4. Prototype S-UEM setup at Sandia consisting of an optical setup coupled into an SEM. A pulsed UV laser is used to generate electron pulses (probe) from the SEM's Schottky field emission filament. The sample is optically excited (pumped) by the same UV laser, which is delayed by a controllable amount, forming the time delay in the multi-pulse pump-probe measurement.

2.1. System overview

The primary components of our S-UEM consist of an optical setup and an SEM. The SEM was modified to accommodate optics for steering and focusing the laser beams, which are coupled in free-space from an optical table adjacent to the SEM.

2.1.1. Optical setup

We use a Fianium HYLASE fiber laser system that provides 10 ps, 1064 nm pulses at variable repetition rates from kHz to 40 MHz. For electron generation and optical excitation, we use the UV third harmonic at 355 nm. We also have the option of using the second harmonic at 532 nm. Our harmonic generation is achieved with an LBO Type I crystal for second harmonic generation (SHG) followed by an LBO Type II crystal for third harmonic generation (THG). Both LBO crystals are 15 mm long, and neither is actively cooled. To improve the conversion efficiency, we use a long focal length lens and position the THG crystal at the focal point. The SHG crystal is placed as close as possible to the THG crystal so that focusing occurs in both.

To simplify alignment, the pump is routed through a motorized delay, rather than the probe. Our motorized stage (Newport IMS1200LM-SA) has a 1200 mm travel range with a minimum incremental motion of 20 nm. We use three retroreflectors to pass the beam four times over the stage length. At some stage position, the path lengths of the pump and probe pulse trains are matched (t = 0), and as the stage length is decreased from there, the pump pulses will precede the probe pulses by greater amounts.

Due to the length of our motorized pump delay, we required a short fixed probe delay to compensate such that t = 0 was within our motorized delay range. The speed of electrons varies with energy, so the position corresponding to t = 0 will depend on the SEM accelerating voltage used (see Figure 12). The long length of our pump delay line makes accelerating voltages from 3-30 kV accessible within our controllable delay range. Furthermore, the length of the fixed probe delay can be easily varied to provide additional time window flexibility.

2.1.2. SEM

We use a Phillips/FEI XL30s SEM, with a thermally-assisted Schottky field emission gun. The sharp filament has a tip radius of ~500 nm, and is comprised of tungsten coated in zirconium oxide, which helps lower the work function. An extraction field of ~4 kV is used. In normal SEM mode, the filament is kept glowing hot (~1800 K) to further decrease the work function and enable ZrO_x to flow down to the filament's apex. In S-UEM mode, we want to minimize thermally emitted electrons, so the current used to Joule heat the filament is turned off and the filament is operated near room temperature.

The SEM column has a viewing window for measuring the filament temperature. We use this existing window to couple in our laser for photoelectron excitation. The line-of-site to the filament through holes in the Wehnelt cylinder is such that the laser impinges on the side of the filament, with the laser path perpendicular to the filament axis. A more favorable angle of attack for photoemission would be to aim the laser up at the apex of the filament, but utilizing the existing optical access window greatly simplified the system, as we avoided modifying the ultra high vacuum gun chamber.

The window material is leaded glass to block x-rays emitted from the gun. We measured ~88% transmission of 355 nm through this window and ~12% transmission of 266 nm, so any future

system that uses the fourth harmonic would likely require replacing the window and proper x-ray shielding.

The conflat flange containing the window protrudes from the SEM and was used to mount a small optical breadboard on the SEM column to accommodate the optics required for steering/focusing the electron generation laser onto the filament. These optics consist of a 355 nm mirror and a 125 mm focal length lens mounted in a 3-axis piezo-controlled stage, as shown in Figure 5. The piezo stage is essential for aligning the laser to the apex of the filament, especially if the SEM is on a floating stage, which causes the precise alignment to fluctuate if a manual micrometer is used. To achieve photoemission, the laser must be sufficiently focused (a fluence of ~1 mJ/cm^2 is needed) and positioned exactly on the apex.

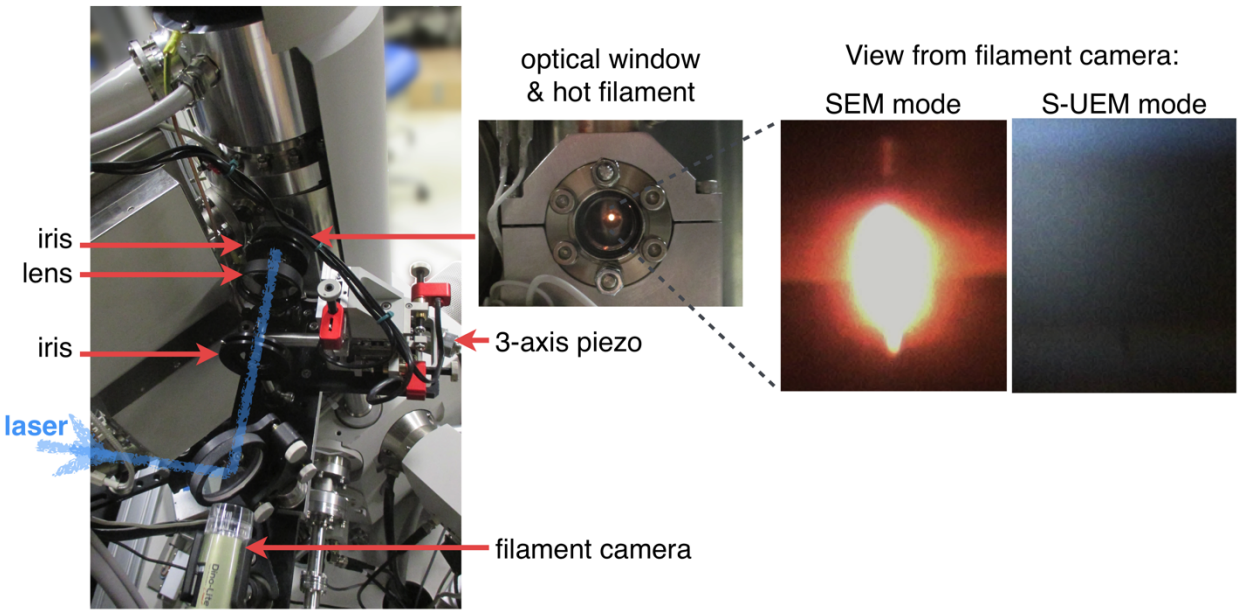

Figure 5. Column-mounted optics for steering and focusing the electron generation laser.

The optical pump is coupled into the SEM through a windowed conflat flange, which was added to an existing port on the sample chamber. Again this conflat is used to mount the optics necessary steering/focusing optics for the pump: a 355 nm mirror and a lens on a manual 3-axis stage. A manual stage is sufficient because the positioning requirement for the pump is less precise, and because after initial alignment, mirrors on the adjacent optical table can be used for fine positioning of the pump to avoid shaking the floating SEM.

To aid in alignment, both optical setups attached to the SEM contain long working distance microscope cameras (Dino-Lite AD4113TL) positioned behind the 355 nm mirrors.

The signal strength in S-UEM depends on the number of electrons per pulse that interact with the sample. The number of SEs ejected for each primary electron is <1. We found that to have

sufficient signal strength during pump-probe operation, we had to use large final apertures on our SEM. Conventional high resolution 30 um diameter apertures resulted in ~0.1 electrons per pulse. Apertures diameters ranging from 100 um to 500 um were used instead.

2.2. Electron probe

Electron pulses are generated through photoemission when the UV generation laser interacts with the cool filament. The work function of the room temperature zirconium oxide coated tungsten filament under the electrostatic extraction field is ~3.3 eV [1], so 355 nm photons (3.49 eV) exceed the work function by a small amount and are capable of exciting photoemission.

For the highest time resolution, Coulomb repulsion between electrons in an electron pulse packet should be minimized. This requires a small number of electrons per pulse [1,20] and a high SEM accelerating voltage. Slow moving electrons have more time to repel each other, so higher accelerating voltages are preferable to minimize the electron packet pulse width. The greatest contribution to packet spreading occurs in the gun, where the electrons are accelerated from their initial energy of <1 eV to ~4 keV.

2.2.1. Alignment procedure for electron generation laser

To achieve a photoexcited electron pulse train, the UV excitation laser must be tightly focused and positioned at the apex of the filament. Figure 6 shows the size of the filament relative to the focused laser beam. The filament is accessed through a hole in the Wehnelt cylinder.

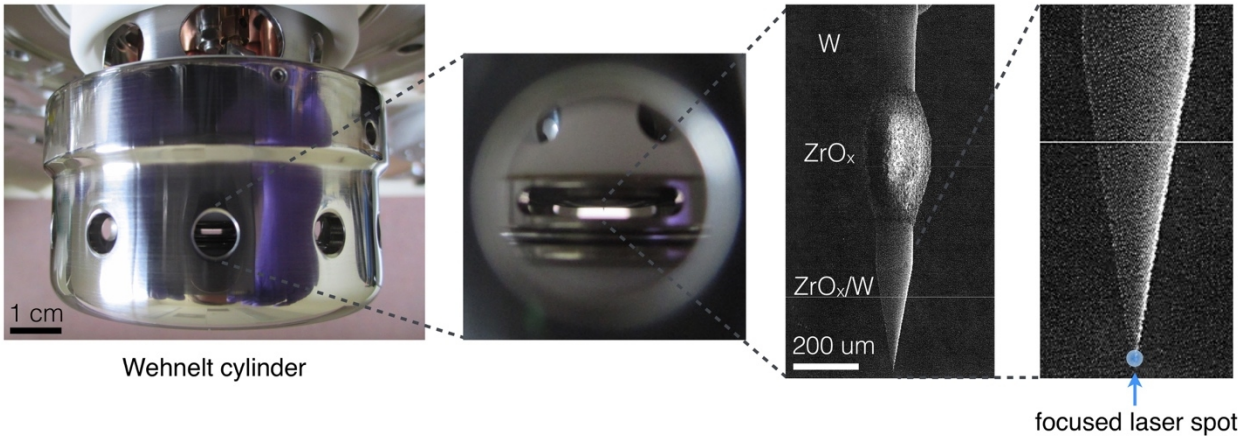

Figure 6. ZrO_x/W filament and illustration of focused laser spot at filament apex. The filament is viewed through a hole in the Wehnelt cylinder. Filament SEM courtesy of Scanservice Inc.

To achieve alignment of the UV laser on the filament apex, we use the optics shown in Figure 5, which are mounted on an optical breadboard affixed to the windowed conflat flange. The use of

a three-axis piezo stage for lens positioning is essential. Attempts with a manual micrometer stage were overly sensitive to motion of the floating SEM table. We describe the initial alignment procedure, assuming that no prior alignment has been done. Once the system has been aligned initially, and in particular once the focal point of the lens has been positioned at the filament axis, then subsequent alignments require more minor adjustments. Because the SEM table is floating and the laser is coupled in free-space, the alignment requires minor adjustments whenever the SEM moves.

For initial course alignment, two irises are centered on the window and used as references to steer the beam towards the filament. The microscope camera behind the mirror is positioned so that it has a straight-on view of the filament through the irises. The lens is roughly positioned by estimating the SEM column radius. The current on the filament is lowered until the filament glow can be barely seen in the microscope camera, as shown in Figure 7a. A low average laser power of 10-20 mW is used at a repetition rate of 10-40 MHz, corresponding to pulse energies of 0.2-2 nJ. The location of the laser beam can be roughly located by moving the lens until the beam hits a metal surface in the Wehnelt cylinder either just above or just below the filament, as shown in Figure 7b. The beam should be roughly focused at this location. Next, the lens is moved to bring the laser onto the filament shaft. The filament will glow brighter due to laser heating, as shown in Figure 7c, and the SE image will become brighter as well. The focus of the lens is now adjusted to maximize the brightness of the glowing filament, or correspondingly the brightness of the SE image. The diameter of the filament is ~150 um, and the maximum brightness due to laser heating will occur when the full laser spot is on the shaft.

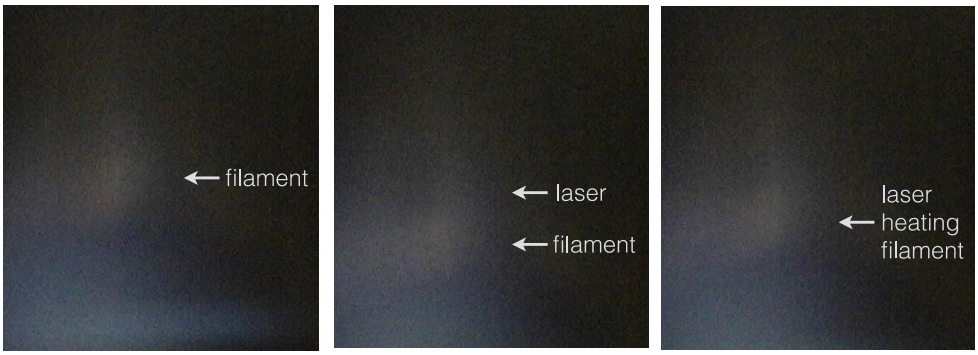

Figure 7. Alignment of the laser on the filament as viewed through the microscope camera. (a) Filament current is reduced until filament is barely visible in microscope camera. (b) Lens is adjusted until laser beam is seen on metal structure directly above filament. (c) Lens is adjusted until laser beam hits filament shaft, which causes filament to glow brighter due to laser heating.

Now that rough focusing of the lens with respect to the filament has been achieved, the beam can be positioned on the apex. The beam is centered horizontally on the shaft by moving it on/off in the horizontal direction until a centered position has been determined. The filament current is now reduced until the SE image is barely visible at full detector contrast (gain). This results in a

minimum background of thermal electrons while maintaining some SE image for alignment feedback. The power of the laser is increased to operational levels of 1-10 nJ/pulse. The beam is now moved vertically down the shaft towards the apex. Minor adjustments to horizontal alignment are made in tandem. As the beam approaches the apex, the SE image may increase in brightness due to increased laser heating near the apex where there is less material, and thus less heat capacity. Once the beam hits the apex, the SE image will become notably brighter due to the contribution from photoemitted electrons, as shown in Figure 8. Note that if the focal point of the lens is far from the axis of the filament, the increase in brightness at the apex may be rather subtle, as fluence scales with the square of beam diameter. For noticeable photoemission, the fluence should be ~1 mJ/cm^2 or more at the apex. As the beam is moved below the apex, the SE image will notably dim, and similarly as the beam is moved above the apex or to either side, the SE image will dim. With the beam at the apex, the focus position of the lens is again adjusted to optimize the SE image brightness. As the waist approaches the filament axis, the horizontal and vertical alignments will become more sensitive and require tweaking to maintain alignment with the apex. Once the SE brightness has been optimized by adjusting the lens position in all three dimensions with the beam at the apex, the current on the filament can be turned all the way down. The system is now operating with a pulse train of photoemitted electrons and very little or no thermally emitted electrons.

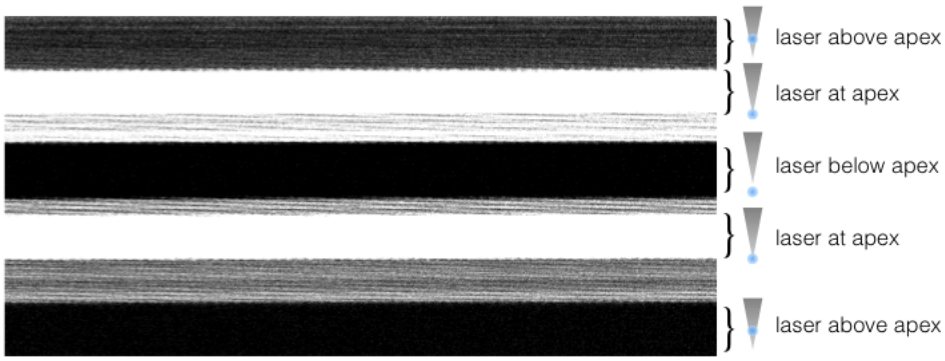

Figure 8. Change in SE image brightness as laser is moved to filament apex. Laser has been well focused on the filament. SE image collected using a 500 um diameter SEM aperture to allow for high primary beam current.

2.2.2. Verifying alignment of electron generation laser

To verify photoemission, three simple tests can be performed. First, if the excitation laser is blocked, the SE image will immediately become dark, as shown in Figure 9a. Second, if the polarization of the excitation laser is rotated, the image will be clear and bright when the laser polarization is parallel to the axis of the filament and dim when the laser polarization is perpendicular to the axis of the filament, as shown in Figure 9b. Photoemission is most efficient with parallel polarization, while thermionic emission is most efficient with perpendicular polarization [24,25]. Lastly, by moving the beam small amounts in the vertical (down off the apex and up the shaft away from the apex) and horizontal directions (off the apex to either side), the SE image will dim as the beam becomes misaligned with the apex.

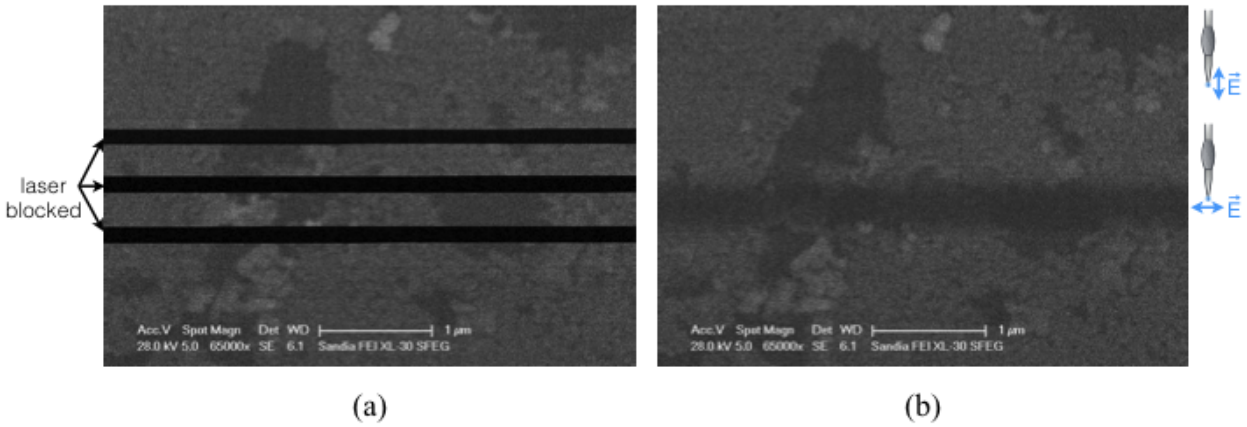

Figure 9. Simple tests to verify photoemission: (a) Blocking the excitation laser immediately and substantially darkens the SE image. (b) Polarization rotation of the excitation laser shows a bright, clear image for a parallel orientation of the electric field with respect to the filament axis and a dim image for a perpendicular orientation.

2.3. Optical pump

The optical pump is used to excite carriers in the semiconductor sample. We use 355 nm (3.49 eV) for our pump, which is above the band gap of many semiconductor materials. The fluence of the pump must be sufficient to excite enough carriers to induce a measureable difference in secondary electron emission in the pumped region verses the un-pumped region of the sample. Indirect band gap materials like Si require higher fluence than direct band gap materials, because the probability for carrier excitation is lower. Literature S-UEM systems have used ~1.5e15 photons/cm^2 pump fluence for Si, and ~1.5e14 photons/cm^2 pump fluence for the direct band gap materials GaAs and CdSe [2,22,23]. Assuming an optical penetration depth of 10 nm, ~1.5e14 photons/cm^2 is 1.5e20 photons/cm^3.

2.3.1. Alignment procedure for the pump laser

The pump laser needs to be focused on the sample in the field-of-view of the SEM. A windowed conflat flange was added to the sample chamber, and steering/focusing optics were mounted to that flange, as shown in Figure 10.

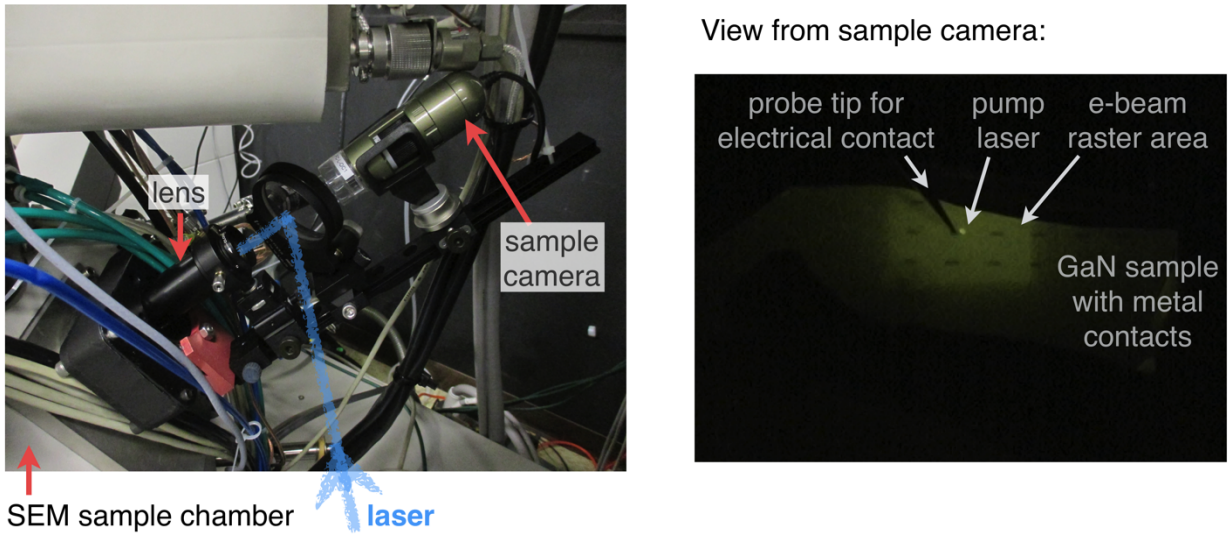

Figure 10. Sample chamber-mounted optics for steering and focusing pump laser.

Initial rough alignment can be accomplished with the sample chamber vented and open. However, when vented, the SEM is no longer supported on floating bearings, so final alignment must be done with the SEM pumped down.

Fine alignment is done with the SEM operating using a luminescent material such as a phosphor or GaN as shown in Figure 10. Under a high primary SEM beam current, the rastering of the SEM beam can be visualized on the sample microscope camera due to the luminescence of the sample material. The position of the pump beam on the sample can also be identified on the microscope camera image. The microscope camera provides sufficient feedback for aligning the pump near the center of the SEM field-of-view as well as approximate focusing.

Even finer adjustment of the pump alignment and focus is accomplished using high pump fluences and low e-beam accelerating voltages. On a variety of samples, the pump can be seen in real-time in the SE image as shown in Figure 11. The pump contrast may be due to laser damage or long-lived near-surface traps. We used this pump visualization method to verify that the pump beam stays stationary as the motorized delay line is swept over its full length.

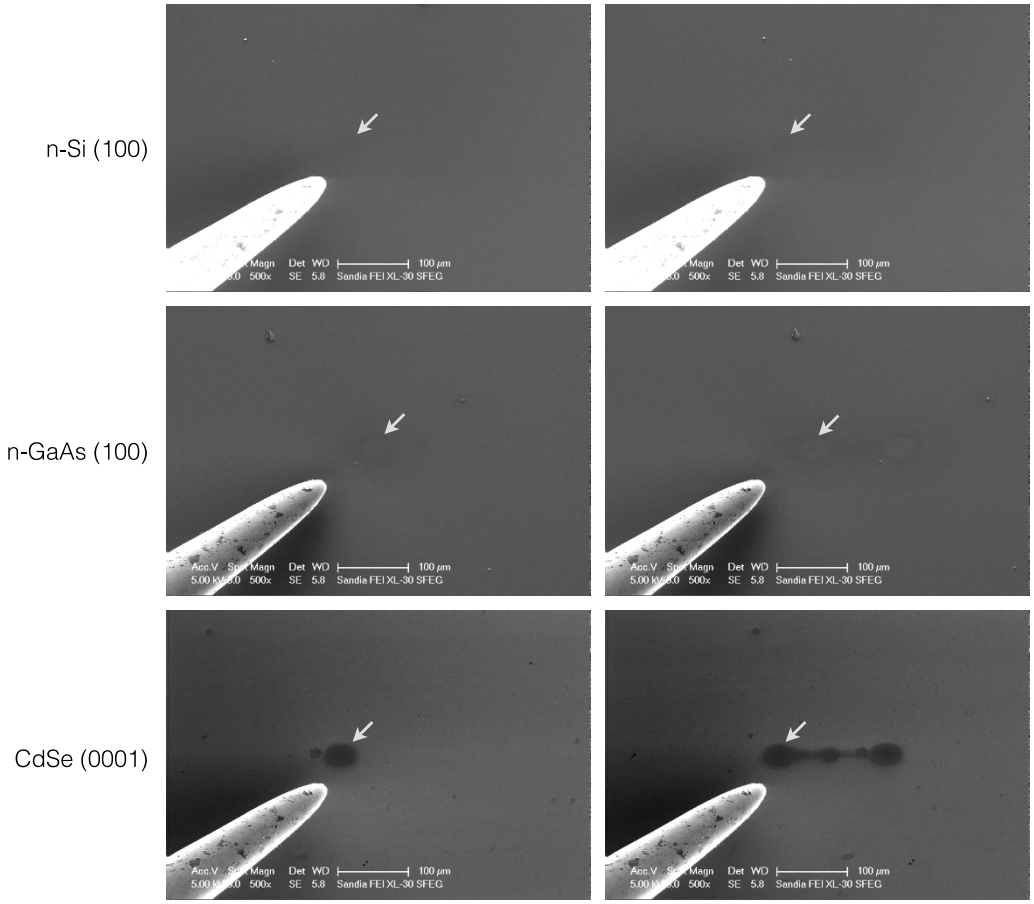

Figure 11. Pump beam apparent in SE contrast for various materials. A full power, continuous e-beam was used with a standard 30 um aperture in conjunction with a 355 nm, 10 ps pump, with a repetition rate of 10 MHz and a pulse energy of 5 nJ. Arrows point to the current pump location. Previous pump location (left column) is still apparent as sample is moved (right column). An electrical contact probe is visible in the lower left, but it is not in contact with the samples.

2.4. Timing

To simplify alignment requirements, we use a motorized delay stage in our pump path rather than in our probe path, as shown in Figure 4. The precision required in aligning the electron generation laser to the filament made a movable delay in the probe path impractical. Instead, we use the movable delay to shorten the pump path length with respect to the probe path length, such that the optical pump pulses arrive before the electron probe pulses.

To match the path lengths of the pump and probe beams, the speed of electrons as they travel down the SEM column must be accounted for. The speed of electrons in vacuum varies with applied field, and is significantly lower than the speed of light. Figure 12 shows a plot of the relativistic speed of electrons at the various accelerating voltages available in our SEM as a fraction of the speed of light.

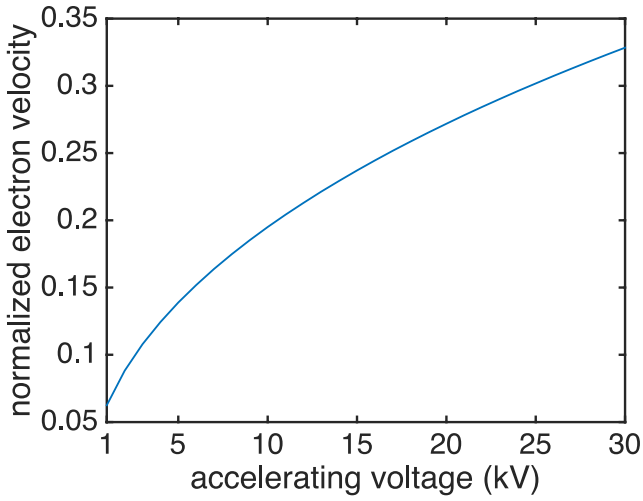

Figure 12. Variation in electron speed as a function of SEM accelerating voltage. Electron velocity is normalized to the speed of light in a vacuum, and accounts for relativistic effects [26].

To find the movable delay position that results in simultaneous arrival of the pump and probe pulses, dubbed t = 0, we first estimated the path lengths with string and a ruler. We carefully measured the distance along the optical paths, starting at the polarizing beam splitter where the pump and probe paths separate (see Figure 4).

To estimate the length of the SEM column, we used a scale column drawing, in addition to coarse estimation. As a first order approximation, we assumed the effective path length of the electrons as they traveled from the filament to the sample would be the filament-to-sample distance (~441 mm) multiplied by the speed of electrons at the chosen accelerating voltage. This is only a rough approximation because electrons do not travel at a constant speed down the column. In the gun, electrons start with a low energy when they are emitted from the filament (<1 eV), and are accelerated to ~4 kV over a short distance. The subsequent electron optics apply various fields to the beam, which all influence the electrons' speed and resulting arrival time. Nevertheless, we found our first order approximation was not far off and allowed us to reasonably estimate for the delay position corresponding to t = 0.

To more accurately determine the delay position corresponding to t = 0, we set up a timing experiment using a fast photodiode (Thorlabs 210) placed at the sample position inside the SEM. We removed the protective window over the diode so that the e-beam could hit the Si diode directly. Figure 13 shows the resulting time-domain oscilloscope traces. We triggered the scope using a second fast photodiode measuring part of the laser. We biased the detector inside the SEM at 12 V, and used a 1 GHz amplifier (Ortec 9327) outside the SEM to enhance the signal entering the scope. With a pulsing e-beam at 30 kV and a 500 um final SEM aperture, we were able to excite a measurable number of electron-hole pairs in the diode, as shown in Figure 13a. The electron pulses have the same pulsing frequency as the laser (20 MHz). Next we excited the diode with our pump laser at various delay positions, as shown in Figure 13b-Figure 13e. Our rough estimation was that t = 0 would be at a delay position of -131 mm at 30 kV. From the

traces, it is apparent that our estimate was not far off. At a delay of 0 mm (Figure 13b), the electron pulses precede the pump pulses, and at a delay of -200 mm, the pump pulses precede the electron pulses, so t = 0 must be between these delays. A delay of 0 mm is the center position of our movable stage, and the stage is variable between -600 mm and 600 mm at a precision of 20 nm. Because we pass the pump four times over the movable delay, 50 mm of delay length corresponds to 667 ps.

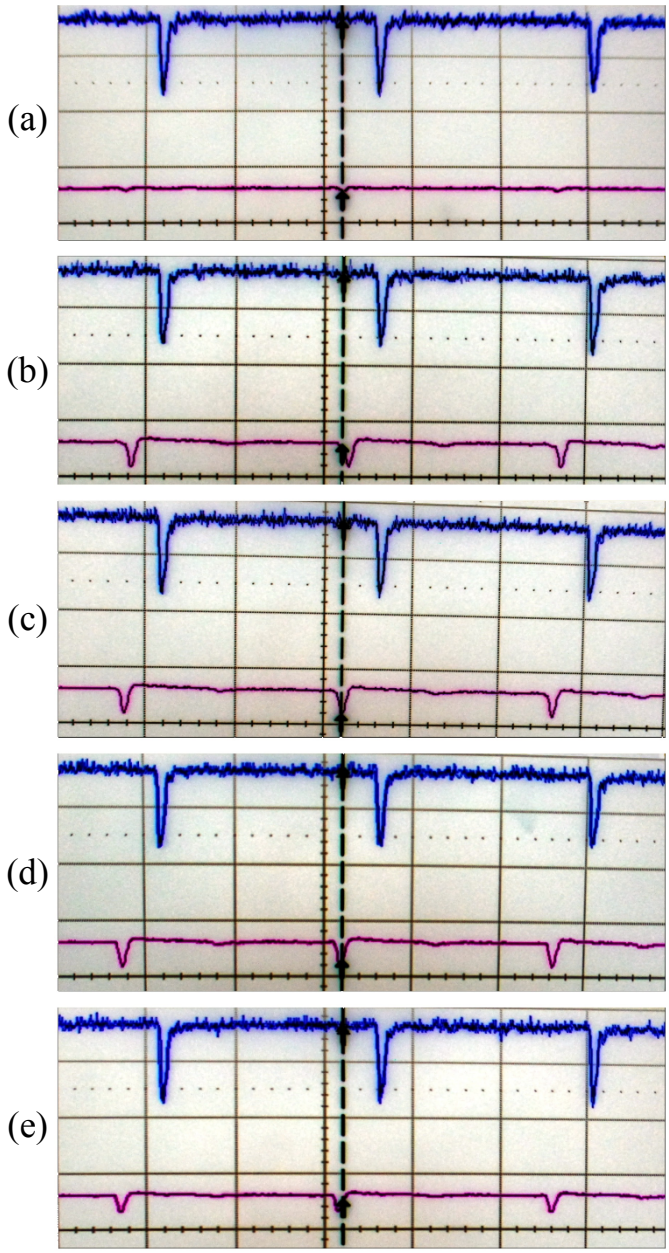

Figure 13. Timing experiment: A fast photodiode is inserted into the SEM at the sample position to visualize the arrival time of the optical pump relative to the electron probe and to estimate the delay position corresponding to t = 0, when the pump and probe arrive simultaneously. Triggering (upper traces) is done with a second photodiode measuring part of the optical beam. (a) Shows electron pulses alone with no optical pump and indicates that the e-beam (lower trace) is pulsing at the laser frequency. (b)-(e) Show pump pulses at delay positions of 0, -100, -150, and -200 mm respectively (lower traces). At a delay of 0 mm (b), electron pulses precede the pump, while at a delay of -200 mm (e), the pump precedes the electron probe, demonstrating that t = 0 lies between 0 and -200 mm.

2.5. System performance

While we have demonstrated that our system produces electron pulses, we have yet to observe good time-resolved SE contrast in the pumped sample area. We believe the primary reason for this is poor signal-to-noise resulting from pump photons being measured by our SE detector. Additionally, improvements to mechanical stability would enable longer dwell times that could aid signal-to-noise. We discuss each of these points further below.

2.6.1. Detection

Given the low number of electrons per pulse, and the even lower number of resulting SEs, the detection efficiency for SEs needs to be high. We are using an Everhart-Thornley scintillator detector mounted inside our sample chamber to measure SEs. This is the standard SE detector that came with the commercial SEM system. The response time of the detector does not need to be fast, since the time resolution in the measurement comes from the delayed arrival of the pump and probe pulses. The detector consists of a P47 phosphor, a light pipe, and a photomultiplier tube (PMT). The detector is not designed to be light-tight inside the sample chamber, as conventional SEM setups have no reason to anticipate the presence of visible light inside the sample chamber during operation. As a result, the detector measures pump photons in addition to SEs, and the much greater number of pump photons overwhelm the detector with background noise.

We are exploring several options for improving our detection setup. One option is to modify the detector by inserting an optical bandpass filter in front of the PMT that will restrict the incoming photons to the phosphor's emission spectrum. However, the high energy of 355 nm photons likely excite emission from P47, which luminesces near 400 nm, so it may be necessary switch to 532 nm for pump excitation.

2.6.2. Stability

The SEM is mounted on a floating table, which is decoupled from the optical table. The laser beams are sent into the SEM from the optical table in free space. Thus, any vibrations of the SEM table cause slight changes to the positioning of the laser beams. This stability issue limits the time scale over which a measurement can be performed. We find we need to adjust the alignment of the excitation laser to the filament apex every 1-3 mins, so we collect S-UEM images in 30-60 s at a given delay position. If the system were more stable, we could increase our image acquisition times, and thus improve imaging resolution.

Several options exist for improving stability. The SEM could be mounted on a vibration isolation system that is less prone to fluctuation, or the SEM and laser setups could be mounted together on a large floating table. Alternatively, the laser beams could be coupled to the SEM through fibers rather than in free space.

2.6. Laser-induced contrast in doped Si

Even without time-resolved imaging, we have observed interesting laser-induced SE contrast effects, as shown in Figure 14 and **Error! Reference source not found.**Figure 15. The sample used was Si with regions of different doping covered in a ~3.5 nm oxide. The e-beam was operated in the usual SEM continuous wave (CW) mode with an accelerating voltage of 5 kV. The pump laser was 355 nm, 10 ps pulses at 10 MHz, with an energy of ~4 nJ/pulse.

Regions of p-Si appear brighter than regions of n-Si in SE imaging even without laser illumination, a phenomena that has been explained through the differences in surface band bending of p- and n-type materials [27]. In p-type materials, the surface bands bend downwards, leading to more SE emission compared to n-type materials, where the surface bands bend upwards [27]. Under laser illumination, we observe bright contrast in both p- and n-type Si regions, as shown in Figure 14. Bright contrast has also been observed in reported time-resolved S-UEM imaging on Si, with brighter contrast in p-type Si, which was attributed p-Si having a larger absorption cross section than n-Si [3]. A greater number of SEs may be emitted from the illuminated region because the laser-excited carriers require less added energy for generating SEs [23].

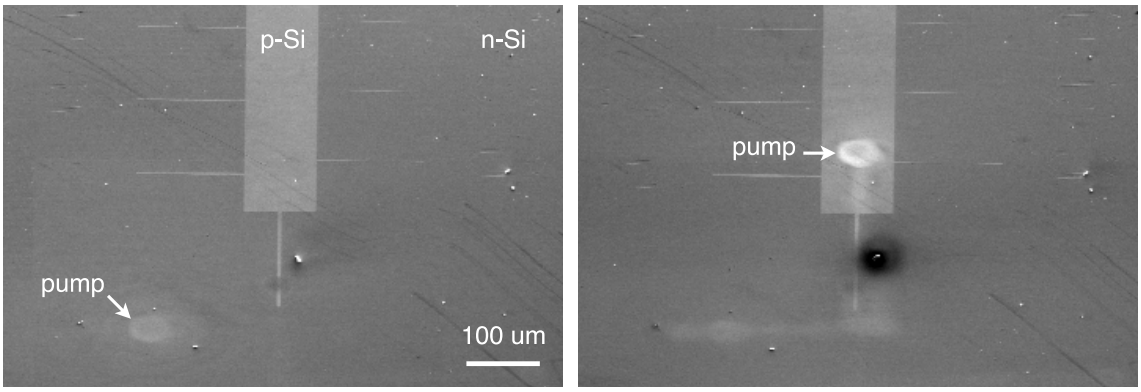

Figure 14. Laser-induced SE contrast in doped Si with CW e-beam. Pump laser produces bright contrast in both n-type (a) and p-type regions.

We also observed doping contrast inversion under laser illumination, as shown in Figure 15. Inversion in doping contrast has been reported for oxide-covered Si by varying e-beam accelerating voltage [28], but to our knowledge this is the first observation of SE contrast inversion due to laser excitation. In the case of contrast inversion by varying e-beam accelerating voltage, the phenomenon was only observed on Si samples with native oxides. Samples where the oxide had been chemically removed did not show contrast inversion, leading the authors to conclude that surface oxygen is an important contributor to SE contrast [28]. Our Si sample that exhibited laser-induced contrast inversion had an oxide of ~3.5 nm. With no laser illumination, an n-type line feature appeared darker than the surrounding p-type area (see Figure 15a). With

laser illumination, the contrast inverted, with the n-Si line becoming brighter than the p-Si surroundings (see Figure 15b). The contrast inversion was apparent both in and near the laser-illuminated region, but far from the laser-illuminated region, the contrast inversion was not apparent. Removing the laser illumination caused the contrast to revert back to the original state (see Figure 15a). One possible explanation for the observed contrast inversion is the reduction of band bending due to photoexcited carriers. In the absence of band bending, n-Si has a lower work function than p-Si, leading to more SE emission from n-Si. Understanding SE doping contrast has attracted great interest as a potential method of determining doped regions in semiconductor devices with nanometer spatial resolutions. Both experimental investigations and theoretical modeling of SE doping contrast are active areas of research [28].

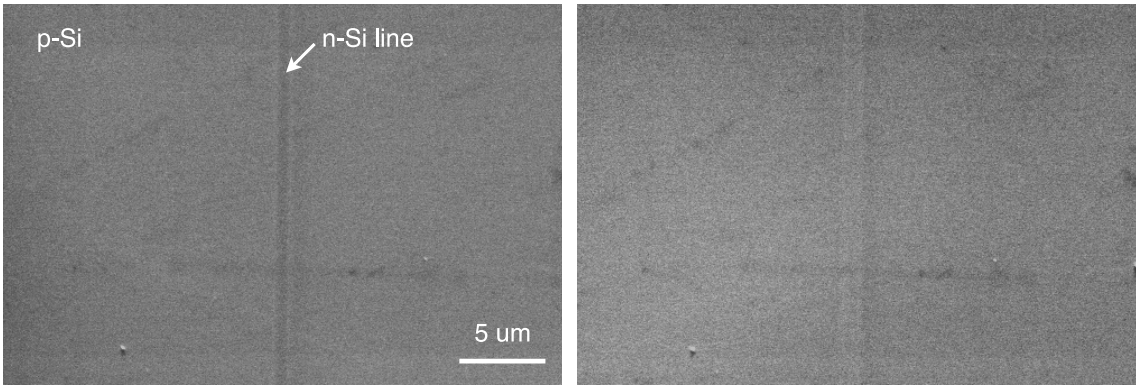

Figure 15. SE contrast inversion of doped Si under laser illumination. (a) With no laser, the CW e-beam SE image shows the n-Si line as darker than the p-Si region. (b) With nearby pump laser illumination, the n-Si line becomes brighter than the surrounding p-Si region, demonstrating laser-induced contrast inversion.

3. SUMMARY AND OUTLOOK

A prototype S-UEM system was constructed, demonstrating the necessary components for stroboscopic optical pump, electron probe measurements in an SEM. We have detailed our S-UEM system components as well as the practical aspects of our implementation. Electron pulse train generation was achieved by pulsed UV laser illumination of a Schottky field-emission filament in a commercial SEM. No modifications to the electron column were required, as the microscope had a built-in optical access window for filament temperature measurements. Electron pulses were verified in real time with a fast photodiode inserted into the SEM at the sample position, and timing of the electron probe with respect to the optical pump was also determined. The secondary electron image does not show good contrast under S-UEM operation, likely due to the contribution of photons to the SE detector signal. Potential strategies for improving signal-to-noise include detector modifications to reject pump photons as well as increasing mechanical stability of the floating SEM relative to the static optical table. Overall, our prototype system proves the principle of S-UEM operation. Further improvements would enable the examination of carrier dynamics in real semiconductor devices.

REFERENCES

[1] D. S. Yang, O. F. Mohammed, and A. H. Zewail, "Scanning ultrafast electron microscopy," *Proceedings of the National Academy of Sciences*, vol. 107, no. 34, pp. 14993-14998, August 2010.

[2] O. F. Mohammed, D. S. Yang, S. K. Pal, and A. H. Zewail, "4D Scanning Ultrafast Electron Microscopy: Visualization of Materials Surface Dynamics," *Journal of the Americal Chemical Society*, vol. 133, pp. 7708-7711, May 2011.

[3] E Najafi, T. D. Scarborough, J. Tang, and A. H. Zewail, "Four-dimensional imaging of carrier interface dynamics in p-n junctions," *Science*, vol. 347, no. 6218, pp. 164-167, January 2015.

[4] D. K. Schroder, *Semiconductor Material and Device Characterization*, 3rd ed.: John Wiley & Sons, 2006.

[5] M. Levinshtein, S. Rumvantsev, and M. Shur, *Handbook Series on Semiconductor Parameters: In 2 Volumes*.: World Scientific, 1996.

[6] K. Kumakura et al., "Minority carrier diffusion length in GaN: Dislocation density and doping concentration dependence," *Applied Physics Letters*, vol. 86, p. 052105, January 2005.

[7] T. Malinauskas et al., "All-optical characterization of carrier lifetimes and diffusion lengths in MOCVD-, ELO-, and HVPE- grown GaN," *Journal of Crystal Growth*, vol. 300, pp. 223-227, January 2007.

[8] S. Hafiz et al., "Determination of carrier diffusion length in GaN," *Journal of Applied Physics*, vol. 117, p. 013106, January 2015.

[9] O. Bostanjoglo and T. Rosin, "Stroboscopic study on ultrasonic activity in electron-microscope," *Mikroskopie*, vol. 32, no. 5-6, p. 190, January 1976.

[10] W. E. King et al., "Ultrafast electron microscopy in materials science, biology, and chemistry," *Journal of Applied Physics*, vol. 97, p. 111101, June 2005.

[11] T. LaGrange et al., "Single-shot dynamic transmission electron microscopy," *Applied Physics Letters*, vol. 89, pp. 044105–044107, July 2006.

[12] T. LaGrange et al., "Approaches for ultrafast imaging of transient materials processes in the transmission electron microscope," *Micron*, vol. 43, pp. 1108-1120, April 2012.

[13] S. Hihath, M. K. Santala, X. Cen, G Campbell, and K. van Benthem, "High speed direct imaging of thin metal film ablation by move-mode dynamic transmission electron microscopy," *Nature Scientific Reports*, vol. 6, p. 23046, March 2016.

[14] T. LaGrange, B. W. Reed, and D. J. Masiel, "Movie-mode dynamic electron microscopy," *Materials Research Society Bulletin*, vol. 40, pp. 22-28, January 2015.

[15] B. J. Siwick, J. R. Dwyer, R. E. Jordan, and R. J. D. Miller, "Ultrafast electron optics: Propagation dynamics of femtosecond electron packets," *Journal of Applied Physics*, vol. 92, no. 3, p. 1643, August 2002.

[16] B. J. Siwick, J. R. Dwyer, R. E. Jordan, and R. J. D. Miller, "An Atomic-Level View of Melting Using Femtosecond Electron Diffraction," *Science*, vol. 302, pp. 1382-1385, November 2003.

[17] M. Harb et al., "Electronically Driven Structure Changes of Si Captured by Femtosecond Electron Diffraction," *Physical Review Letters*, vol. 100, p. 155504, April 2008.

[18] G. Sciaini and R. J. D. Miller, "Femtosecond electron diffraction: heralding the era of atomically resolved dynamics," *Reports on Progress in Physics*, vol. 74, p. 096101, August 2011.

[19] V. A. Lobastov, R. Srinivasan, and A. H. Zewail, "Four-dimensional ultrafast electron microscopy," *Proceedings of the National Academy of Sciences*, vol. 102, no. 20, pp. 7069-7073, March 2005.

[20] A. H. Zewail and J. M. Thomas, *4D Electron Microscopy: Imaging in Space and Time*.: World Scientific, 2010.

[21] J. Sun, V. A. Melnikov, J. I. Khan, and O. F. Mohammed, "Real-Space Imaging of Carrier Dynamics of Materials Surfaces by Second-Generation Four-Dimensional Scanning Ultrafast Electron Microscopy," *The Journal of Physical Chemistry Letters*, vol. 6, pp. 3884-3890, September 2015.

[22] D. S. Yang, O. F. Mohammed, and A. H. Zewail, "Environmental Scanning Ultrafast Electron Microscopy: Structural Dynamics of Solvation at Interfaces," *Angewandte Chemie International Edition*, vol. 52, pp. 2897-2901, 2013.

[23] J. Cho, T. Y. Hwang, and A. H. Zewail, "Visualization of carrier dynamics in p(n)-type GaAs by scanning ultrafast electron microscopy," *Proceedings of the National Academy of Sciences*, vol. 111, no. 6, pp. 2094-2099, January 2014.

[24] P. Hommelhoff, Y. Sortais, A. Aghajani-Talesh, and M. A. Kasevich, "Field Emission Tip as a Nanometer Source of Free Electron Femtosecond Pulses," *Physical Review Letters*, vol. 96, p. 077401, February 2006.

[25] B. Barwick et al., "Laser-induced ultrafast electron emission from a field emission tip," *New Journal of Physics*, vol. 9, p. 142, May 2007.

[26] University of Oklahoma. Accelerating Voltage Physics Calculator. [Online]. http://www.ou.edu/research/electron/bmz5364/calc-kv.html

[27] I. Volotsenko et al., "Secondary electron doping contrast: Theory based on scanning electron microscope and Kelvin probe force microscopy measurements," *Journal of Applied Physics*, vol. 107, p. 014510, January 2010.

[28] C. G. H. Walker, F. Zaggout, and M. M. El-Gomati, "The role of oxygen in secondary electron contrast in doped semiconductors using low voltage scanning electron microscopy," *Journal of Applied Physics*, vol. 104, p. 123713, December 2008.

DISTRIBUTION

1	MS0359	D. Chavez, LDRD Office	1911
1	MS0620	Meredith Dyck	5644
1	MS0885	Michael Valley	1810
1	MS0886	Blythe Clark	1819
4	MS0886	Joseph R. Michael	1800
1	MS0887	Terrence Aselage	1800
1	MS0889	Wahid Hermina	1850
1	MS1072	Edward I. Cole	1000
1	MS1202	Reid S. Bennett	5957
1	MS 9054	David Chandler	8300
1	MS9054	Sarah Allendorf	8350
4	MS9161	Kimberlee Chiyoko Collins	8342
4	MS9161	Albert Alec Talin	8342
1	MS9161	Christian Mailhiot	8340
1	MS0899	Technical Library	9536 (electronic copy)


Sandia National Laboratories